

Improved Repeatability of the Estimation of Pulsatility of Inferior Vena Cava

*Original*

Improved Repeatability of the Estimation of Pulsatility of Inferior Vena Cava / Mesin, L.; Giovino, T.; D'Alessandro, S.; Roatta, S.; Raviolo, A.; Chiacchiarini, F.; Porta, M.; Pasquero, P.. - In: ULTRASOUND IN MEDICINE AND BIOLOGY. - ISSN 0301-5629. - STAMPA. - 45:10(2019), pp. 2830-2843. [10.1016/j.ultrasmedbio.2019.06.002]

*Availability:*

This version is available at: 11583/2757872 since: 2021-09-08T19:13:16Z

*Publisher:*

Elsevier USA

*Published*

DOI:10.1016/j.ultrasmedbio.2019.06.002

*Terms of use:*

This article is made available under terms and conditions as specified in the corresponding bibliographic description in the repository

*Publisher copyright*

Elsevier postprint/Author's Accepted Manuscript

© 2019. This manuscript version is made available under the CC-BY-NC-ND 4.0 license  
<http://creativecommons.org/licenses/by-nc-nd/4.0/>. The final authenticated version is available online at:  
<http://dx.doi.org/10.1016/j.ultrasmedbio.2019.06.002>

(Article begins on next page)

# Improved repeatability of the estimation of pulsatility of inferior vena cava

Luca Mesin<sup>a,\*</sup>, Tatiana Giovino<sup>a</sup>, Simone D'Alessandro<sup>a</sup>, Silvestro Roatta<sup>b</sup>, Alessandro Raviolo<sup>c</sup>, Flavia Chiacchiarini<sup>c</sup>, Massimo Porta<sup>c</sup>, Paolo Pasquero<sup>c</sup>

*<sup>a</sup>Mathematical Biology and Physiology, Department of Electronics and Telecommunications, Politecnico di Torino, Torino, Italy*

*<sup>b</sup>Integrative Physiology Lab, Department of Neuroscience, University of Torino, Torino, Italy*

*<sup>c</sup>Department of Medical Sciences, University of Torino, Torino, Italy*

---

## Abstract

The inferior vena cava (IVC) shows variations of cross-section over time (pulsatility) induced by different stimulations (e.g., breathing and heartbeats). Pulsatility is affected by patients volume status and can be investigated by ultrasound (US) measurements. An index of IVC pulsatility based on US visualization and called caval index (CI) was proposed as a non-invasive indirect measurement of the volume status. However, its estimation is not standardized, operator-dependent and affected by movements of the vein and non-uniform pulsatility. We introduced a software that processes B-mode US video-clips to track IVC movements and estimate CI on an entire portion of the vein. This method is here compared to the standard approach in terms of repeatability of the estimated CI, reporting on the variability over differ-

---

\*Corresponding Author: Luca Mesin, Dipartimento di Elettronica e Telecomunicazioni, Politecnico di Torino, Corso Duca degli Abruzzi, 24 - 10129 Torino - Italy; Email, luca.mesin@polito.it; Phone, +39 011.090.4085

ent respiratory cycles, longitudinal IVC sections and intra/inter observers. Our method allows to reduce the variability of CI assessment, making a step toward its standardization.

*Keywords:* Inferior vena cava, Ultrasound, Tracking, Repeatability, Volume status

---

## 1 Introduction

2 Pulsatility of the diameter of the inferior vena cava (IVC), estimated from  
3 ultrasound (US) measurements, is a non-invasive procedure, widely adopted  
4 to assess the intravascular volume status both in healthy subjects and con-  
5 ditions of altered volemic status in patients. Specifically, the pulsations of  
6 the vessel visualized by US measurements during the respiratory cycle are  
7 used to estimate the caval index (CI, Blehar et al. (2012)). However, mea-  
8 surement techniques are not standardized (Wallace et al. (2010)), as they  
9 vary in terms of anatomical approach and sonographic technique (Finnerty  
10 et al. (2017)). For example, both recordings along longitudinal (Barbier et al.  
11 (2004); Brennan et al. (2006); Fields et al. (2011); Feissel et al. (2004); Grant  
12 et al. (1980); Kircher et al. (1990); Lyon et al. (2005); Moreno et al. (2019);  
13 Pasquero et al. (2015)) or transversal sections (Blehar et al. (2009); Chen  
14 et al. (2010); Moreno et al. (2019)) of the vein are used. Different recom-  
15 mendations have been proposed on where to measure the vein diameter along  
16 a longitudinal section (Wallace et al. (2010); Resnick et al. (2011)). How-  
17 ever, since the pulsatility of the vessel is not uniform along its longitudinal  
18 axis (Mesin et al. (2015, 2019b)), CI values vary considerably in the litera-  
19 ture in both healthy and pathologic conditions and, as a result, diagnostic  
20 recommendations are also non homogeneous (Zhang et al. (2014)).

21 The movements of the vein relative to the transducer during the respi-  
22 ratory cycle give an additional contribution to the variability of CI. Indeed,  
23 M-mode registration allows to compute the vein diameter along a fixed line  
24 at the end of inspiration and expiration, but, since the IVC moves during  
25 respiration, the diameters end up being taken at different points, introduc-

26 ing a possible bias. This is particularly relevant if the vein has an irregular  
 27 shape, with a variable cross-sectional area (Lichtenstein (2005)) or if the an-  
 28 gle between the M-mode line and the vein changes considerably during its  
 29 movements. In addition, respiration cycles may differ between each other  
 30 and change among subjects (e.g., breathing can be diaphragmatic, thoracic  
 31 or a combination of both), inducing changes in the IVC dynamics (Kimura  
 32 et al. (2011)). In order to minimize movements of the vein during respira-  
 33 tion, variations of the IVC section was investigated during voluntary apnoea,  
 34 thus bringing forward the effect of cardiac activity on IVC pulsatility (Folino  
 35 et al. (2017); Nakamura et al. (2013)), which is otherwise poorly detectable  
 36 on M-mode representation. However, this technique cannot be easily applied  
 37 in clinics.

38 We reported on successfully tracking IVC movements in long-axis US  
 39 scans while estimating its diameter in each frame, along a direction mov-  
 40 ing together with the vein (Mesin et al. (2015)). This method has a lower  
 41 computational cost than other advanced processing techniques applied to US  
 42 images (Yang et al. (2008); Yeung et al. (1998); Krupa et al. (2007)) and pro-  
 43 vides a more precise estimation of the IVC local pulsatility with respect to  
 44 standard measurements, based on a fixed M-mode line (Mesin et al. (2015)).  
 45 However, a possible problem is that pulsatility along a single section of the  
 46 IVC may be not representative of the dynamics of the whole vessel. Some  
 47 parts of the vein are anchored to nearby structures (e.g., the diaphragm or  
 48 vein inlets) and show smaller pulsatility than other portions. For example,  
 49 lower pulsatility was reported at the level of the diaphragm compared to  
 50 more caudal sites (Wallace et al. (2010)). These observations were confirmed

51 in Mesin et al. (2015) (Figure 9), showing that diameter variations along  
 52 distinct directions (moving together with the vein) resulted in considerably  
 53 different pulsatility. Lack of consensus about where to measure diameters  
 54 (Wallace et al. (2010); Resnick et al. (2011)) and the non-uniform behaviour  
 55 of the vessel are likely to contribute to the non-homogeneous assessments  
 56 of IVC pulsatility in the literature (Weekes et al. (2012)). Thus, we re-  
 57 cently proposed a new algorithm that tracks the movements and computes  
 58 the diameter of different sections of a whole portion of the IVC (Mesin et al.  
 59 (2019b)). In this study, we compare this innovative method to the standard  
 60 approach, in terms of the repeatability (intra- and inter-operator) of infor-  
 61 mation extracted from different measurements on the same subjects. The  
 62 repeatability of IVC assessment by the standard technique was investigated  
 63 in a few contributions in the literature (Fields et al. (2011); Finnerty et al.  
 64 (2017)). The measurement of the diameter was found to be reliable, but the  
 65 assessment of IVC pulsatility was quite poor (Fields et al. (2011)). The sub-  
 66 xifoideal transabdominal long axis view in B-mode demonstrated the highest  
 67 inter-rater reliability (Finnerty et al. (2017)) among different anatomical ap-  
 68 proaches, including also the transabdominal short axis immediately inferior  
 69 to the inflow of the hepatic veins and the right lateral transabdominal coronal  
 70 long axis. Here, the possibility of tracking the IVC and examining an entire  
 71 portion of the vein allowed us to investigate different sources of variability in  
 72 the US assessment, including different respiration cycles, sections along the  
 73 longitudinal axis, experimental sessions and operators.

## 74 **Materials and Methods**

### 75 *Automated detection of the IVC borders*

76 US video-clips were processed using the algorithm proposed in Mesin  
77 et al. (2019b), which allows to obtain a continuous measurement of IVC  
78 borders along an entire portion of the vessel after compensating for possible  
79 movements. The algorithm was implemented in MATLAB R2018a (The  
80 Mathworks, Natick, Massachusetts, USA).

81 The user is asked to indicate the location of the vein in the first frame  
82 (Figure 1A). Moreover, as shown in Figure 1B, on the same frame, he chooses  
83 two reference points to be tracked (to account for IVC movements and de-  
84 formations) and the most proximal/distal sections (defining the portion of  
85 the IVC of interest, which was between the confluence of the hepatic veins  
86 into the IVC and the caudate lobe of the liver). Finally, the locations of the  
87 borders of the vein along the most proximal line are indicated. The software  
88 is then ready to process the video-clip. It distributes uniformly  $N$  lines in  
89 the portion of IVC indicated by the user ( $N=21$  in this paper) and automat-  
90 ically detects the borders of the vein along these lines (as points for which an  
91 abrupt change of intensity is found; Figure 1C). For each frame, the location  
92 and direction of the  $N$  lines are updated depending on the movements of the  
93 reference points (specifically, in general the segment joining the two reference  
94 points is found slightly translated, rotated and scaled in subsequent frames;  
95 the  $N$  lines are translated and rotated and their distribution is updated ac-  
96 cordingly, so that in different frames they are ideally fixed on same sections  
97 of the vein). In this way, the superior and inferior borders of the vein are  
98 estimated in the IVC portion of interest (see Mesin et al. (2019b) for details).

## 99 *Subjects*

100 US data were recorded from 10 healthy volunteers (5 females, 5 males;  
101 mean $\pm$ std age  $30\pm 13$  years, height  $172\pm 12$  cm, weight  $63\pm 11$  kg) with a  
102 SonoSite M-Turbo system (SonoSite, Bothell, USA; frame rate 30 Hz, reso-  
103 lution of about 0.42 mm per pixel, 256 gray levels) equipped with a convex 2-5  
104 MHz probe. Two-dimensional (B-mode) longitudinal views of the IVC were  
105 taken with a subxifoideal approach (as suggested by Finnerty et al. (2017)),  
106 with the subject in the supine position during relaxed normal breathing.  
107 The study was approved by the Ethics Committee of the University of Turin  
108 and complies with the principles of the Declaration of Helsinki. All subjects  
109 provided written informed consent for the collection of data and subsequent  
110 analysis.

## 111 *Experimental set-up and protocol*

112 The experimental protocol is illustrated in Figure 2. Three operators  
113 performed the US scans: one expert (PP), one in training (AR) and one be-  
114 ginner (FC), with balanced arrangement of their order. An operator started  
115 by taking 3 measurements of IVC diameters (as defined below) using standard  
116 methodology in M-mode. Then, a 15s video-clip was recorded in B-mode,  
117 allowing for at least three respiratory cycles. After the first recording, the  
118 subject was asked to stand up for one minute to minimize any changes of  
119 the IVC due to remaining in the supine position for a prolonged time (Folino  
120 et al. (2017)). Then, the subject was asked to lie down again supine and a  
121 new acquisition was taken by a second operator and, after standing up again,  
122 by a third one. The whole procedure was repeated a second time, obtaining  
123 six video-clips for each subject.



## 124 *Indexes extracted from the data*

125 Different indexes were taken from each measurement, in order to test their  
126 repeatability. Three manual measurements in M-mode were taken before  
127 registering the video-clips. The operator chose three respiratory cycles. For  
128 each of them, the maximum and minimum vein diameters ( $D_{max}$  and  $D_{min}$ ,  
129 respectively) were indicated, and the (manual) CI was computed as

$$CI = \frac{D_{max} - D_{min}}{D_{max}} \quad (1)$$

130 The video-clips were then processed to estimate the IVC borders as detailed  
131 above. Notice that the position of each point of the border is indicated by  
132 time series (location along  $x$  and  $y$  directions, one value per frame). These  
133 time series were low pass filtered with a 4 Hz cut-off, in order to remove high  
134 frequency and quantization noises (this filter and the ones mentioned below  
135 were of Butterworth type, order 4 and used in both directions to remove  
136 phase distortion and delay, Mesin et al. (2019b)). Then, the borders of the  
137 IVC were estimated from the confluence of the hepatic veins into IVC to 4  
138 cm in distal direction (Figure 1D). Specifically, from the estimated borders,  
139 the IVC midline was computed. It was then approximated by a parabolic  
140 function. The location of the confluence of the hepatic veins into the IVC was  
141 indicated by the user (SA, who was not an echographer) on the first frame of  
142 the video-clip. This point was orthogonally projected on the IVC midline and  
143 represented the starting point from which other 4 points were automatically  
144 estimated, with 1 cm curvilinear distance from each other along the IVC  
145 midline. Thus, 5 points were obtained, 0 to 4 cm distant from the confluence  
146 of the hepatic veins into the IVC, projected on the midline of the vein.

147 Then, the sections orthogonal to the IVC midline passing from each such  
 148 points were considered (Mesin et al. (2019b); Pasquero et al. (2015)) and  
 149 the IVC diameters in these sections were computed by interpolation from  
 150 the estimated vein borders (see Mesin et al. (2019b) for details). These five  
 151 diameters are further considered in the following.

152 The pulsatility of the IVC in each section was described by the (auto-  
 153 mated) CI, defined as

$$CI_{auto} = \frac{\max(D) - \min(D)}{\max(D)} \quad (2)$$

154 where  $D$  indicates the estimated diameter time series (in a specific section).  
 155 Local maxima and minima were computed for each respiration cycle (Figure  
 156 3A). Thus, an estimate of CI was obtained for each respiratory cycle and  
 157 for each section considered. As in the case of the manual CI estimation,  
 158 the CIs of 3 respiratory cycles were selected. In the cases in which more  
 159 than 3 cycles were present in the video-clip, the CIs closer to their mean  
 160 across different cycles were selected. After testing the repeatability across  
 161 respiration cycles, the estimated CIs were averaged. A CI accounting for the  
 162 overall pulsatility of the considered portion of the vein was also considered  
 163 (indicated as  $CI_{global}$ ): it was obtained by averaging the estimates across  
 164 different sections.

165 Additional indexes of pulsatility were obtained after further processing  
 166 the diameter time series estimated by our software. The vein dynamics was  
 167 considered as the sum of two components, reflecting the stimulation induced  
 168 by respiration and heartbeat (Mesin et al. (2019a)). The two components  
 169 were separated as follows: the effect of respiration was computed by low  
 170 pass filtering the whole diameter time series with a cut-off frequency of 0.4

171 Hz. The cardiac contribution was computed by high pass filtering the whole  
 172 diameter time series with a cut-off frequency of 0.8 Hz. Then, the following  
 173 additional indexes were estimated, as shown in Figure 3.

- 174 • The respiratory caval index (RCI), applying the same formula (2) to  
 175 the respiration component only.
- 176 • The cardiac caval index (CCI), applying the same formula (2) to the  
 177 cardiac component only.

178 Also for these two indexes, stimulation cycles were selected: 3 respiration  
 179 cycles and 10 heartbeats were included. Moreover, the subscript global  
 180 was added to indicate their average across different sections ( $RCI_{global}$  and  
 181  $CCI_{global}$ ).

#### 182 *Assessment of repeatability and discriminability*

183 Different indicators were used to assess the repeatability of each index  
 184 (manual and automated CI, CCI, RCI) extracted from the 6 measurements  
 185 performed by the operators.

- 186 • Coefficient of variation (CoV), defined as the ratio between the stan-  
 187 dard deviation and the mean of the estimates. It was used to test  
 188 variations due to different respiration cycles, sections and experimental  
 189 sessions (intra- and inter-operator).
- 190 • Intraclass correlation coefficient (ICC). It is defined as

$$ICC = \frac{var(S)}{var(S) + var(M) + var(E)} \quad (3)$$

191 where  $var(S)$ ,  $var(M)$  and  $var(E)$  indicate the variability due to dif-  
192 ferent subjects, measurements (i.e., experimental sessions) and residual  
193 error, respectively (Bartko (1966)). It was used to test intra- and inter-  
194 operator variability.

195 An index of discrimination was also employed, to test the possibility that  
196 an index could be repeatable, but not able to distinguish between different  
197 subjects. The Fisher ratio was used. It measures the linear discrimination  
198 between two sets of values as

$$FR = \frac{(\mu_1 - \mu_2)^2}{\sigma_1^2 + \sigma_2^2} \quad (4)$$

199 where  $\mu_k$  and  $\sigma_k^2$  (with  $k = 1, 2$ ) are the mean and the variance of the  $k^{th}$  sets,  
200 respectively. The sets to be compared were constituted by the 6 values of  
201 a specific index extracted from the different measurements on each subject.  
202 The mean of the Fisher ratios measuring the discrimination of each pair of  
203 subjects was used as overall discriminability indicator.

204 Finally, the different sources of variability were investigated by analysis of  
205 variance (ANOVA). The manual CI and  $CI_{global}$  were processed with a 4-way  
206 ANOVA (normality of residuals was assessed by Lilliefors test), investigating  
207 the variability induced by the following factors: subject (10 individuals),  
208 operator (3 levels), repetition (2 levels) and respiration cycle (3 cycles).

209 Some paired tests for significant variations among couples of variables  
210 were also performed, using Wilcoxon signed rank tests. The significance  
211 level was set to  $p = 0.05$ .

## 212 *Summary of investigated indexes*

213 The following indexes are considered.

- 214 1. Manual CI, which is a variable depending on the following factors: res-  
 215 piration cycle (3 cycles considered), subject (10 volunteers) and experi-  
 216 mental session (6 sections, which could be further split into 3 operators  
 217 repeating twice the experiment). The average across the respiration  
 218 cycles was also considered.
- 219 2.  $CI_{auto}$ ,  $RCI_{auto}$  and  $CCI_{auto}$ , depending on the following factors: respi-  
 220 ration cycle (3 cycles considered) or heartbeat in the case of  $CCI_{auto}$   
 221 (10 beats considered), subject, section (5 locations, measured in terms  
 222 of the distance from the hepatic veins) and experimental session. The  
 223 average across the respiration cycles/heartbeats was also considered.
- 224 3.  $CI_{global}$ ,  $RCI_{global}$  and  $CCI_{global}$ , obtained by averaging the previous in-  
 225 dexes across the sections (obtaining a global index for the vein tract  
 226 under study), so that they depend on respiration cycle or heartbeat (the  
 227 latter in the case of  $CCI_{global}$ ), subject and experimental session. The  
 228 average across the respiration cycles/heartbeats was also considered.

## 229 Results

230 Figures 4-7 show different contributions to the variability of the estimates  
 231 of some indexes reflecting the pulsatility of IVC. For clarity, a single source  
 232 of variability is considered in each figure (respiration, longitudinal section,  
 233 experimental session and intra-/inter-operator variability, respectively) and  
 234 only some indexes are shown. The whole database is fully explored with the  
 235 statistical analysis shown in Tables 1-3.

236 *Variability of CI in subsequent breaths*

237 Figure 4A shows the changes in IVC diameter exhibited in a representa-  
238 tive subject at rest. The tracings refer to different IVC sections (simultane-  
239 ously monitored in the same video-clip), located at 0, 2 and 4 cm distal to the  
240 confluence of hepatic veins into the IVC. Notice that the sections exhibit dif-  
241 ferent average diameter and different amplitude of oscillatory components of  
242 cardiac and respiratory origin. For example, at the confluence of the hepatic  
243 vein, the algorithm estimated different respiration cycles with CIs varying  
244 in the range 18%-28% and with a CoV equal to 19%. This CoV indicates  
245 the variability of the CI estimations across the different respiration cycles  
246 (recorded in the same video-clip, at a location fixed to the IVC). Figure 4B  
247 shows the distribution of these CoVs extracted from the whole dataset. This  
248 CoV, expressing the variability observed over consecutive respiratory cycles,  
249 was calculated for all trials (obtaining 60 values, as we considered 10 sub-  
250 jects for 6 experimental sessions) and for each IVC section. In addition, for  
251 comparison, the same figure also includes the CoV of  $CI_{global}$  and  $CI_{manual}$ .  
252 Notice that the median variability with respect to different respiration cycles  
253 (in terms of CoV) is about 15% when considering the standard (manual)  
254 method, about 5% when considering single sections ( $CI_{auto}$ ) tracked by the  
255 automated method (Mesin et al. (2019b)) and lower than 3% when consider-  
256 ing the global CI (averaged over all IVC sections,  $CI_{global}$ ; Wilcoxon signed  
257 rank test indicates that the CoV of manual and global CI are statistically  
258 different).

259 *Variability of CI with longitudinal position*

260 For all the following figures, CI estimations (either manual or automated)  
261 were derived as the average of the values obtained from the different respi-  
262 ratory cycles.

263 Figure 5 shows the variability of CI estimation across different sections  
264 along the IVC. The dependence of IVC pulsatility along the longitudinal  
265 position is visible in 5A for the different subjects ( $CI_{auto}$  is shown averaged  
266 over all 6 experimental sessions). Notice that there is no univocal trend in  
267 CI dependence on longitudinal position. The variations of CI in different  
268 positions can be relevant: e.g., in subject number 7,  $CI_{auto}$  decreases from  
269 about 40% to 10%, moving caudally by 3 cm from the confluence of the  
270 hepatic veins into IVC; conversely, in subject 8, CI increases from about 50%  
271 to 70%, over the same distance.

272 The variability of  $CI_{auto}$  along the considered IVC tract was quantified by  
273 its CoV. One estimation of CoV was obtained for each experimental session,  
274 obtaining 6 values for each subject which are shown in Figure 5B. On average,  
275 it is about 30%, but it is as high as about 70% in one subject (number 7 in  
276 Figure 5B).

277 *Variability of CI, RCI and CCI over the different experimental sessions*

278 For the different indexes (now including also RCI and CCI), the CoV  
279 was computed over the 6 experimental sessions, thus providing a measure of  
280 repeatability of the assessment for each subject.

281 This evaluation was conducted separately for the different positions along  
282 the IVC in order to compare automated and manual assessments. As il-  
283 lustrated in Figure 6, none of the sections along the IVC exhibits a CoV

284 significantly smaller than the others. Moreover, it can be observed that i)  
 285 manual and automated assessments (over single sections) have similar vari-  
 286 ability (6A); ii) removing the respiratory component improves repeatability  
 287 (6B and 6D); iii) filtering out the cardiac component does not improve re-  
 288 peatability (6C and 6D); iv) a relevant reduction in CoV of  $CI_{auto}$  is obtained  
 289 by calculating the CI over the entire longitudinal portion of IVC ( $CI_{global}$ ).  
 290 Statistically significant differences were found between  $CCI_{global}$  and manual  
 291 CI,  $CI_{global}$  and  $RCI_{global}$ ,  $CCI_{global}$  and  $RCI_{global}$ .

#### 292 *Intra- and inter-operator variability of CI assessment*

293 Figure 7 shows a comparison between the CoV of manual CI and global  
 294 automated estimation ( $CI_{global}$ ). Intra-operator variability was computed us-  
 295 ing the two repetitions of the measurement by the specific operator consid-  
 296 ered. Inter-operator variability was computed from the average CI obtained  
 297 by the operators (averaging the two repeated measurements) from each sub-  
 298 ject. The spread of the estimates obtained from the same subject was lower  
 299 for the automated method for 9 subjects out of 10 (Wilcoxon signed rank  
 300 test indicated that the automated method provided estimates of CI from the  
 301 same subject with lower standard deviations than the manual approach; the  
 302 CoV of manual and global CI were not statistically different, instead). Most  
 303 of the repeated manual measurements of each operator were quite similar  
 304 (mean intra-operator CoV equal to 28%), but the estimations varied a lot  
 305 among different operators (mean inter-operator CoV equal to 35%). The  
 306 automated measurements were more stable and showed similar intra- and  
 307 inter-operator variabilities (mean CoV equal to 24% and 18%, respectively).



### 308 *Repeatability assessment*

309 The figures discussed in the previous sections considered single sources  
310 of variability (respiration cycle, longitudinal section, experimental session  
311 and operator in Figures 4, 5, 6 and 7, respectively). Here, the statistical  
312 analysis of the entire dataset is discussed. Table 1 shows the ANOVA, com-  
313 paring the manual CI and  $CI_{global}$ . Notice that the total variability of CI  
314 is larger when using the standard clinical approach. Moreover, as indicated  
315 by the F statistics, a slightly higher percentage variability is obtained con-  
316 sidering different subjects when using the automated method instead of the  
317 standard one (so that a better discrimination of different subjects can be  
318 obtained using the automated algorithm). On the other hand, a lower vari-  
319 ability is obtained using the automated method in different experimental  
320 sessions (when pooling together the factors repetition and operator, results  
321 not shown) and respiration cycles (even if the variations induced by the res-  
322 piration cycle are not significant). Splitting the experimental sessions into  
323 the factors repetition and operator, we notice that the variations on different  
324 repetitions are quite small (and not significant), whereas larger (significant)  
325 differences are found considering different operators (in line with the intra-  
326 and inter-operator CoV discussed above). Moreover, smaller variations over  
327 different repetitions are found for the standard approach, whereas those in-  
328 duced by different operators are smaller for the automated approach. Thus,  
329 the automated method provided measurements that were more stable across  
330 different operators, whereas, by the standard approach, the echographers ob-  
331 tained twice similar values, which were however different from those of the  
332 colleagues, indicating a possible bias.

333 Tables 2 and 3 show respectively the ICC and the Fisher ratio of the caval  
 334 indexes computed either by the standard or the automated method (manual  
 335 CI,  $CI_{global}$ ,  $CCI_{global}$  and  $RCI_{global}$ ). Intra-operator values were computed  
 336 considering only the estimates obtained by each operator, separately; inter-  
 337 operator values were obtained by grouping together the estimates of the  
 338 same operator. Notice that the most experienced operator obtained quite  
 339 high values of ICC and Fisher ratio, considering both the standard method  
 340 and the indexes extracted from the video-clips that he recorded. The CIs  
 341 measured with the standard method had a correlation with those estimated  
 342 by our software using the corresponding video-clips (i.e., those registered after  
 343 the M-mode assessment) which was found to be related to the experience:  
 344 FC, AR and PP (i.e., the operators in order of increased experience) showed a  
 345 correlation coefficient of 36.2%, 58.1% and 70.8%, respectively (the definition  
 346 of correlation coefficient is

$$C = \frac{\sum_n (x[n] - \bar{x})(y[n] - \bar{y})}{\sqrt{\sum_n (x[n] - \bar{x})^2 \sum_m (y[m] - \bar{y})^2}} \quad (5)$$

347 where  $x[n]$ ,  $y[n]$  are the series to be compared and  $\bar{x}$ ,  $\bar{y}$  are their means).  
 348 Notice that the estimates of CI obtained by the automated method are more  
 349 consistent across different operators (inter-operator ICC about 70%, whereas  
 350 it is about 61% for the standard estimation). High values of ICC were ob-  
 351 tained also for the estimation of CCI, lower values for RCI (in line with  
 352 Figure 6). Notice also that the video-clips acquired by the most experienced  
 353 operator allowed to get more repeatable estimates of the automated indexes  
 354 (this indicates the importance of acquiring good video-clips to get repeatable  
 355 results also from the automated processing). The results on ICC are in line

356 with those shown by the Fisher ratio (Table 3): indeed, a larger repeatability  
357 of the estimation of pulsatility of each subject allows to better discriminate  
358 between different subjects.

## 359 Discussion

### 360 *Summary*

361 Repeatability of standard CI estimations was assessed in a group of  
362 healthy subjects, the results indicating rather poor values in terms of both  
363 intra- (mean CoV=28%, ICC in the range 49-82%) and inter-operator vari-  
364 ability (mean CoV=41%, ICC=61.5%). These results are in line with the  
365 previous studies in the literature (Fields et al. (2011); Finnerty et al. (2017)).  
366 For example, Fields et al. (2011) reported a high inter-rater reliability of IVC  
367 diameter estimation, but a lower repeatability of pulsatility assessment, with  
368 ICC very similar to ours.

369 Here, we propose the use of a semi-automated algorithm, analysing 15s  
370 lasting B-mode video-clips of the IVC acquired with the subxifoideal ap-  
371 proach in long axis (which demonstrated the highest inter-rater reliability,  
372 Finnerty et al. (2017)). We found

- 373 1. some variability of the CI over the respiratory pattern (CoV about 5%,  
374 whereas it is about 15% for the standard approach),
- 375 2. high variability of the CI depending on the longitudinal site of assess-  
376 ment (median of CoV ranging among 10 and 70% for different subjects,  
377 after averaging across respiration cycles).

378 Since the choice of the insonation point and the breath cycle is arbitrary,  
379 these factors can induce a variability between different measurements. In the

380 present work, we attempted to limit these sources of variability mediating  
381 estimations obtained from different breath cycles and on a 4 cm portion of  
382 the IVC in long axis. Due to this averaging, in addition to the tracking of  
383 the vein movements (with reliability already proven in Mesin et al. (2015)),  
384 the algorithm offers a more objective and reliable measurement of the CI  
385 (here called global CI), reducing the overall variability (intra- and inter-  
386 operator mean CoV equal to 24% and 18%, respectively; ICC=70.4%). The  
387 inter-rater reliability of the estimation of the CI is higher than that found  
388 using the standard approach. It is also higher than the one reported in  
389 the literature (Fields et al. (2011); Finnerty et al. (2017)), even if healthy  
390 eu-volemic subjects were considered (in the literature, improvement in inter-  
391 rater reliability was found when assessing hyper- and hypo-volemic patients  
392 Fields et al. (2011); Finnerty et al. (2017)). In addition, the identification  
393 of the respiratory and the cardiac oscillatory components may provide new  
394 insights and possibilities for the analysis of IVC dynamics, with repeatability  
395 performances close to those of the standard CI and global CI, respectively.

#### 396 *Discussion of different sources of variability*

397 The pulsatility of the IVC by the CI estimation is widely used to assess the  
398 volemic status in different clinical conditions. However, the measurements  
399 are not standardized and the recommendations given in the literature are  
400 not univocal (Zhang et al. (2014)).

401 The repeatability of the estimation of the IVC pulsatility has been inves-  
402 tigated in few studies (Fields et al. (2011); Finnerty et al. (2017)). It is a very  
403 important information, as low repeatability hampers clinical usefulness. For  
404 the problem at hand, it reflects an uncertainty that limits the discrimination

405 of the volume status of different patients and the reliability in the follow up.  
406 In this paper, we report low repeatability of classical CI assessment, investi-  
407 gate relevant sources of variability and propose a method that improves the  
408 measurement. Specifically, the following sources of variability were explored.

- 409 • The variation of the depth and modality of respiration induces different  
410 IVC pulsatility for each breath cycle. Notice that controlling the res-  
411 piration cycle (e.g., by a spirometer, even if only the respiration depth,  
412 not the modality, could be controlled) could possibly reduce this source  
413 of variability. Indeed, in the case of mechanically ventilated patients,  
414 the respiration cycles are regular and the dynamics of the IVC diame-  
415 ter was found to be useful to detect fluid responsiveness (Feissel et al.  
416 (2004)). To overcome the variability induced in spontaneous breathing,  
417 the analysis of cardiac pulsatility has been proposed: pulsatility was  
418 measured during a short apnoea, thus caused by the heartbeats only  
419 (Folino et al. (2017); Nakamura et al. (2013)).
- 420 • Variations of the pulsatility in different sections of the vein. These  
421 variations were noticed both in longitudinal (Mesin et al. (2015, 2019b))  
422 and transversal scans (Blehar et al. (2012)).
- 423 • Variations introduced by the operator. In different measurements, the  
424 investigated 2D section can be slightly different. Furthermore, the US  
425 probe handled by the operator must follow the movements of the pa-  
426 tient during respiration: the ability to follow the movement without  
427 affecting the measurement depends on the level of experience of the  
428 operator.

429 In addition, there are variations of the investigated IVC section, due to move-  
 430 ments of the vein during an M-mode measurement (as the M-mode registra-  
 431 tion fixes the considered section in space). Consider that both translation  
 432 and rotation of the vein with respect to the studied direction are expected  
 433 to occur in general. The former induces an error in the estimated diameter  
 434 dependent on the shape of the vein, while rotation affects the estimated di-  
 435 ameter even if the vein is a perfect cylinder. The problem is reflected by an  
 436 error in the estimation of pulsatility, which depends on the range of move-  
 437 ments and anatomy of the vein (Mesin et al. (2015)). In this paper, such  
 438 a problem affected only manual estimations. The automated IVC tracking  
 439 (introduced in Mesin et al. (2015, 2019b)) allows to remove this source of  
 440 uncertainty.

441 The other three sources of variation mentioned above were investigated  
 442 in this study, considering both the standard manual measurements and the  
 443 automated estimations provided by the algorithm proposed in Mesin et al.  
 444 (2019b), which estimates the IVC sections in a whole portion of the vein.  
 445 Figures 4-7 show repeatability in terms of CoV, so that the variation is  
 446 measured as the standard deviation of the estimates normalized with respect  
 447 to their mean.

- 448 • The CI (as a measurement of IVC pulsatility) in different respiration  
 449 cycles had median variation which was about the 15% and 5% or 3%  
 450 of the mean value, for the manual and the automated methods respec-  
 451 tively, either considering a single section or averaging across a portion  
 452 of the vein (Figure 4). A large variability among different subjects was  
 453 observed, with the largest variations being about the 90% and the 30%,

for the manual and the global automated method (averaging across sections), respectively. The repeatability is much larger for the automated method than considering the clinical standard. For the following discussion, this variability was removed considering the average CI among respiration cycles (for both the manual and the automated method).

- A large variation of CI was observed when considering different sections along the IVC (Figure 5), confirming that the vein pulsations vary a lot, depending on anatomical properties of the vein and of the surrounding tissues (e.g., the presence of anchoring sites). The sections were studied using the automated method, which tracked their motion. The average CoV was about 40%, with great variations among subjects (the one showing the largest differences among sections showed a CoV of about 70%). No section can be considered better than others in terms of repeatability of the estimations: the best one varies among the subjects and also considering different measurements on the same subject. Moreover, a large variability of CI was observed among subjects, without a clear trend of pulsatility when going in proximal or distal direction along the considered longitudinal section of the IVC (extending 4 cm distal from the confluence of the hepatic veins). The great variability of IVC pulsatility along the cranio-caudal direction can lead to misinterpretation of the overall dynamics of the IVC.
- Considering the measurements of different echographers, we observed a large variability, both among experimental sections (Figure 6) and intra-/inter-operators (Figure 7). The operators had different expe-

478 rience: more than 20 years (PP), 2 years (AR) and less than 1 year  
479 (FC). Their procedures in taking the manual measurements were quite  
480 different.

- 481 – PP tried to select a direction orthogonal to the IVC midline (Pas-  
482 quero et al. (2015)). On average, the measuring site was 2.4 cm  
483 from the confluence of the hepatic veins, i.e., close to the centre  
484 of the considered portion of IVC.
- 485 – AR took the measurement quite close to the diaphragm, on aver-  
486 age 1.7 cm from the confluence of the hepatic veins (25% of times,  
487 the measuring site was at a distance from the confluence of the  
488 hepatic veins lower than 1 cm). This procedure helped him in  
489 getting stable measurements in different experiments, as there are  
490 anatomical references which could be easily found. However, in  
491 that region, the vein pulsatility is affected by anchoring tissues  
492 and the blood flow from the hepatic vein, so that the accuracy of  
493 the measurement could be questionable.
- 494 – FC showed a lower experience than the colleagues, as her measure-  
495 ments required longer time and efforts. On average, the measuring  
496 site was 2.7 cm from the confluence of the hepatic veins and the  
497 distribution of chosen sites was the most dispersed among the col-  
498 leagues (std of about 1.4 cm, whereas it was 0.94 and 1.15 for PP  
499 and AR, respectively).

500 The ANOVA allows to interpret the different sources of uncertainty in CI  
501 estimation and to assess the intra- and inter-operator variability. Our re-



502 sults suggest that the operators had a different consistent bias when taking  
 503 measurements following the standard procedure. Indeed, their intra-operator  
 504 estimates were quite consistent (mean CoV=28%), but differed from those  
 505 of their colleagues (inter-operator CoV=35%). This possibly reflects the dif-  
 506 ferent preferred measurement sites of the operators (so that the longitudinal  
 507 section is similar for the repeated measurements, but different among the  
 508 three operators). The automated approach, when compared to the stan-  
 509 dard one, provided smaller variability (mainly inter-operator), suggesting  
 510 that it could contribute to standardizing CI measurements (intra-operator  
 511 and inter-operator mean CoV equal to 24% and 18%, respectively). Fur-  
 512 thermore, the average ICC and Fisher ratio were higher in the CI estimated  
 513 by the automated method, suggesting that the new approach may allow to  
 514 better discriminate different subjects. Finally, comparing the standard and  
 515 automated CI estimations, a direct correlation emerged with operators' expe-  
 516 rience (the lowest and highest correlation for the least and most experienced  
 517 echographer, respectively). Hence, the automated method could also be a  
 518 reference for teaching to novices how to make a manual measurement.  
 519 A real time rendering of the identified IVC borders could be a useful feed-  
 520 back to guide the acquisition of a B-mode video-clip. Notice also that the  
 521 most experienced operator (who made measurements highly correlated to  
 522 those of the automated method) selected the M-mode line along the direc-  
 523 tion mostly orthogonal to the IVC midline: our results further support this  
 524 choice, already suggested in Pasquero et al. (2015).

525 *RCI and CCI: new indexes estimated by the automated method*

526 As the automated method provides not only local estimates, but time  
527 series, more information can be extracted by post-processing. Specifically,  
528 the respiratory and cardiac oscillatory components were separated and addi-  
529 tional indexes (RCI and CCI) were computed. Figure 6 shows that RCI has a  
530 larger variability than CCI. It is reasonable that the variability is lower when  
531 considering an index reflecting the cardiac instead of the breath stimulation.  
532 Indeed the effect of the heartbeats is about constant, whereas the respiration  
533 cycles can be more variable, so that their effect on different measurements  
534 can be important. Moreover, the number of heartbeats is much larger than  
535 that of respiration cycles found in the same video-clip, so that more estima-  
536 tions can be averaged when computing CCI than RCI.

537 Notice that the CoV of the RCI is larger than that of the automated esti-  
538 mation of the CI ( $CI_{global}$ ), even if the latter is affected by the asynchronous  
539 super-position of the heartbeats over the respiration cycles, which introduces  
540 a variation in the estimations. However, even if the variability of the estima-  
541 tions of CI is a bit larger than that of the RCI, the mean value is much lower  
542 for the latter than the first, so that its CoV is larger. A similar interpreta-  
543 tion can be given concerning the results of CCI: the estimates are very stable  
544 (with a much lower variability than that of CI), but their absolute values are  
545 very small. However, CCI is the index providing the largest ICC (Table 2)  
546 and Fisher ratio (Table 3), indicating that it has high repeatability and can  
547 better discriminate different subjects. Further work is needed to understand  
548 how the information provided by these two indexes correlate with the state  
549 of the patient (this work investigates only the repeatability of their estima-

550 tions). For example, we expect that irregular cardiac rhythm may cancel or  
551 largely affect the cardiac component, so that the relative weight of the two  
552 components could be of help in discriminating some patients.

### 553 *General comments*

554 The consequence of the large variability of the standard measurement  
555 is that clinical CI estimations should be considered with caution (Magnino  
556 et al. (2017)). Indeed, problems are expected when the index is used to  
557 discriminate between patients with different pathologies: for example, only  
558 differences among subjects in the order of 20-30% can be assessed with some  
559 confidence. Moreover, it is difficult to monitor a patient in the follow up,  
560 as only large variations can be assessed. Finally, clinicians using different  
561 approaches in selecting the M-mode line could get different diagnoses.

562 In order to improve the reliability and repeatability of the estimations,  
563 a possible solution is averaging more measurements. Different CIs measured  
564 on more respiration cycles can be averaged. In this way, an index is obtained  
565 accounting for different vein dynamics, induced by different breath stimula-  
566 tions. Moreover, averaging allows to reduce estimation errors due to small  
567 mistakes in measuring on still images the maximal and minimal diameters  
568 (also affected by the asynchronous summation of heartbeats and respiration  
569 cycles). Furthermore, an average of information from different sections could  
570 further improve the estimation of IVC pulsatility, at the expense of spending  
571 time repeating more M-mode investigations along different sections.

572 Our method allows to estimate and average information from different  
573 respiration cycles and sections automatically, processing a single US video-  
574 clip. This provides a fast and robust overall estimation of the pulsatility in

575 an entire portion of the vein. Here, we show that the averaged estimation  
576 provided by our semi-automated method is also more repeatable than the  
577 manual assessment.

578 Our results could be considered preliminary, due to the low number of  
579 investigated subjects (i.e., 10). However, other indications of the reliability  
580 of the information extracted by our automated algorithm are available. For  
581 example, the pulsatility of IVC extracted by our algorithm has been recently  
582 used to estimate the right atrial pressure, with performances largely superior  
583 than those that could be obtained from the manual estimations (Mesin et al.  
584 (2019a)). Moreover, works are in progress on the applications on patients,  
585 where our algorithm allows to get better discrimination of patients affected  
586 by either hypo- or hyper-volaemia.

587 Using an automated method reduces the problems due to subjective in-  
588 terpretations. However, the procedure is still dependent on the quality of the  
589 video recorded by the operator, so that the experience of the echographer is  
590 still important. In future, the real time rendering of the output of the pro-  
591 cessing algorithm could provide a feedback to help the operator to acquire  
592 a video-clip of good quality. Even considering this limitation of our work  
593 (in which the processing was executed off-line), our algorithm allowed to get  
594 CI estimations closer to those obtained by the most experienced operator,  
595 also when applied to video-clips recorded by a low experience echographer.  
596 Thus, we propose this innovative algorithm as a step towards standardizing  
597 measurements of IVC pulsatility.

598 An instrument applying the algorithm described in this paper was patented  
599 by Politecnico di Torino and Università di Torino (patent number 102017000006088).

## 600 **Conclusions**

601     Different sources of variability affect the estimation of IVC pulsatility  
602 from US measurements, e.g., the respiration cycles and the selected section  
603 of the vein. Our semi-automated algorithm allows to track vein movements  
604 and deformations in long axis, to compute the diameter of different sections  
605 orthogonal to the vein and to provide an estimation of pulsatility which is  
606 averaged across respiration cycles and sections. The pulsatility estimations  
607 of this software were found to be more repeatable than those obtained by  
608 the standard approach. This method can provide a contribution in the stan-  
609 dardization of the assessment of IVC pulsatility, with important outcomes  
610 expected in the estimation of the central venous pressure and volemic status  
611 of patients.

612 **References**

- 613 Barbier C, Loubieres Y, Schmit C, Hayon J, Ricome J, Jardin F. Vieillard-  
614 Baron A. Respiratory changes in inferior vena cava diameter are helpful in  
615 predicting fluid responsiveness in ventilated septic patients. *Intensive Care*  
616 *Med*, 2004;30:1740-1746.
- 617 Bartko J. The intraclass correlation coefficient as a measure of reliability.  
618 *Psychol Report*, 1966;19:3-11.
- 619 Blehar D, Dickman E, Gaspari R. Identification of congestive heart failure  
620 via respiratory variation of inferior vena cava diameter. *Am J Emerg Med*,  
621 2009;27:71-75.
- 622 Blehar D, Resop D, Chin B, Dayno M, Gaspari R. Inferior vena cava dis-  
623 placement during respirophasic ultrasound imaging. *Critical Ultrasound*  
624 *Journal*, 2012;4:1-5.
- 625 Brennan J, Ronan A, Goonewardena S, Blair J, Hammes M, Shah D, Vasai-  
626 wala S, Kirkpatrick J, Spencer K. Handcarried ultrasound measurement of  
627 the inferior vena cava for assessment of intravascular volume status in the  
628 outpatient hemodialysis clinic. *Clin J Am Soc Nephrol*, 2006;1:749-753.
- 629 Chen L, Hsiao A, Langan M, Riera A, Santucci K. Use of bedside ultra-  
630 sound to assess degree of dehydration in children with gastroenteritis. *Acad*  
631 *Emerg Med*, 2010;17:1042-1047.
- 632 Feissel M, Michard F, Faller J, Teboul J. The respiratory variation in infe-  
633 rior vena cava diameter as a guide to fluid therapy. *Intensive Care Med*,  
634 2004;30:1834-1837.

635 Fields J, Lee P, Jenq K, Mark D, Panebianco N, Dean A. The interrater re-  
636 liability of inferior vena cava ultrasound by bedside clinician sonographers  
637 in emergency department patients. *Acad Emerg Med*, 2011;18:98–101.

638 Finnerty N, Panchal A, Boulger C, Vira A, Bischof J, Amick C, Way D,  
639 Bahner D. Inferior vena cava measurement with ultrasound: What is the  
640 best view and best mode? *West J Emerg Med*, 2017;18:496–501.

641 Folino A, Benzo M, Pasquero P, Laguzzi A, Mesin L, Messere A, Porta  
642 M. Roatta S. Vena cava responsiveness to controlled isovolumetric res-  
643 piratory efforts. *Journal of Ultrasound in Medicine*, 2017;36:2113–2123.

644 Grant E, Rendano F, Sevinc E, Gammelgaard J, Holm H, S. G. Normal  
645 inferior vena cava: caliber changes observed by dynamic ultrasound. *AJR*  
646 *Am J Roentgenol*, 1980;135:335–338.

647 Kimura B, Dalugdugan R, Gilcrease G, Phan J, Showalter B, Wolfson T.  
648 The effect of breathing manner on inferior vena caval diameter. *Eur J*  
649 *Echocardiogr*, 2011;12:120–123.

650 Kircher B, Himelman R, Schiller N. Noninvasive estimation of right atrial  
651 pressure from the inspiratory collapse of the inferior vena cava. *Am J*  
652 *Cardiol*, 1990;66:493–496.

653 Krupa A, Fichtinger G, Hager G. Full motion tracking in ultrasound using im-  
654 age speckle information and visual servoin. *Proc. ICRA*, 2007:2458–2464.

655 Lichtenstein D. *Inferior vena cava. general ultrasound in the critically ill*.  
656 Berlin: Springer, 2005;23:82.

657 Lyon M, Blaivas M, Brannam L. Sonographic measurement of the inferior  
658 vena cava as a marker of blood loss. *Am J Emerg Med*, 2005;23:45–50.

659 Magnino C, Omedé P, Avenatti E, Presutti D, Iannaccone A, Chiarlo M,  
660 Moretti C, Gaita F, Veglio F, Milan ARI. Inaccuracy of right atrial  
661 pressure estimates through inferior vena cava indices. *Am J Cardiol.*,  
662 2017;120:1667–73.

663 Mesin L, Albani S, Sinagra G. Non-invasive estimation of right atrial pres-  
664 sure using the pulsatility of inferior vena cava. *Ultrasound Med Biol*,  
665 2019a;45:1331–1337.

666 Mesin L, Pasquero P, Albani S, Porta M, Roatta S. Semi-automated tracking  
667 and continuous monitoring of inferior vena cava diameter in simulated and  
668 experimental ultrasound imaging. *Ultrasound Med Biol*, 2015;41:845–857.

669 Mesin L, Pasquero P, Roatta S. Tracking and monitoring of pulsatility of a  
670 portion of inferior vena cava from long axis ultrasound imaging. *Ultrasound*  
671 *Med Biol*, 2019b;45:1338–1343.

672 Moreno F, Hagan A, Holmen J, Pryor T, Strickland R, Castle C. Non-invasive  
673 estimation of right atrial pressure using the pulsatility of inferior vena cava.  
674 *Am J Cardiol*, 2019;53:579–585.

675 Nakamura K, Tomida M, Ando T, Sen K, Inokuchi R, Kobayashi E, Naka-  
676 jima S, Sakuma I, Yahagi N. Cardiac variation of inferior vena cava: new  
677 concept in the evaluation of intravascular blood volume. *J Med Ultrasonics*,  
678 2013;40:205–209.



679 Pasquero P, Albani S, Sitia E, Taulaigo A, Borio L, Berchialla P, Castagno F,  
 680 Porta M. Inferior vena cava diameters and collapsibility index reveal early  
 681 volume depletion in a blood donor model. *Crit Ultrasound J.*, 2015;7:17.

682 Resnick J, Cydulka R, Platz E, Jones R. Ultrasound does not detect early  
 683 blood loss in healthy volunteers donating blood. *J Emer Med.*, 2011;41:270–  
 684 275.

685 Wallace D, Allison M, Stone M. Inferior vena cava percentage collapse during  
 686 respiration is affected by the sampling location: an ultrasound study in  
 687 healthy volunteers. *Acad Emerg Med*, 2010;17:96–99.

688 Weekes A, Lewis M, Kahler Z, Stader D, Quirke D, Norton H, Almond C,  
 689 Middleton D, Tayal V. The effect of weight-based volume loading on the  
 690 inferior vena cava in fasting subjects: a prospective randomized double-  
 691 blinded trial. *Acad Emerg Med.*, 2012;19:901–907.

692 Yang L, Georgescu B, Zheng Y, Meer P, Comaniciu P. 3d ultrasound tracking  
 693 of the left ventricles using one-step forward prediction and data fusion of  
 694 collaborative trackers. *Proc. IEEE Conf Comput Vis Pattern Recognit*,  
 695 2008.

696 Yeung F, Levinson S, Fu D, Parker K. Feature-adaptive motion tracking of  
 697 ultrasound image sequences using a deformable mesh. *IEEE Trans. Med.*  
 698 *Imaging*, 1998;17:945–956.

699 Zhang Z, Xu X, Ye S, Xu L. Ultrasonographic measurement of the respiratory  
 700 variation in the inferior vena cava diameter is predictive of fluid respon-

701 siveness in critically ill patients: Systematic review and meta-analysis.  
702 Ultrasound Med Biol, 2014;40:845–853.

703 **Figure Captions**

704 **Figure 1:** A) Selection of a rectangle including the IVC portion of interest in  
705 the first frame of the video-clip. B) Reference points (squares), leftmost  
706 and rightmost sections of interest (continuous lines) and points close  
707 to the vessel edges along the leftmost section (indicated by X). C)  
708 The algorithm computes 21 lines uniformly distributed between the  
709 extreme sections indicated in B) and estimates the profile of the vein  
710 along them (the estimated border points are indicated with circles). D)  
711 From the estimated border of the vessel, the midline is computed and  
712 interpolated with a parabola (dash-dot line); five equidistant points are  
713 selected on this parabola, starting from the confluence of the hepatic  
714 vein in the IVC and new lines perpendicular to it are considered as  
715 sections along which to compute the vein diameters (border points  
716 indicated with diamonds).

717 **Figure 2:** Experimental protocol. Each operator acquired three manual  
718 measurements (in M-mode) and then the video (in B-mode). The same  
719 procedure was followed twice for each of the three operators.

720 **Figure 3:** A) Caval index (CI) estimated on the whole signal. The local  
721 maxima and minima of the respiratory component are found; then a  
722 window of 1 s duration centred on each of these points is explored  
723 to find the maxima or minima on the whole signal (indicated with  
724 circles). B) Respiratory caval index (RCI), computed on the breath  
725 component. This component is isolated with a low pass filter; then,  
726 maxima and minima (indicated with circles) are automatically found

727 and used for RCI calculation. C) Cardiac caval index (CCI) computed  
728 on the heartbeat component. The component is isolated with a high  
729 pass filter; then, its local maxima and minima (indicated with circles)  
730 are computed and used for CCI estimation.

731 **Figure 4:** A) Time course of IVC diameter at three different sections si-  
732 multaneously monitored in a representative subject. B) Distribution  
733 of CoV of  $CI_{auto}$ , obtained considering the 6 measurements from all 10  
734 subjects, separately for the five sections and compared with manual CI  
735 and  $CI_{global}$ .

736 **Figure 5:** Variation of the Caval Index (CI) when estimated by the au-  
737 tomated method at different longitudinal positions, expressed as the  
738 distance from the confluence of the hepatic veins. A) Each trace cor-  
739 responds to one subject (average of all sessions). B) Median, quartiles  
740 and range (outliers shown individually) of the coefficient of variation  
741 (CoV) of the CI across the 5 sections along the vein, for each subject.

742 **Figure 6:** Coefficient of variation (CoV) for each index (manual CI and au-  
743 tomated estimation of CI, CCI and RCI) computed across different  
744 experimental sessions (median, quartiles and range; outliers shown in-  
745 dividually). A), B) and C): CoV of the indexes (CI, CCI and RCI,  
746 respectively) extracted at different distances from the confluence of the  
747 hepatic vein into the IVC and, to the right, the CoV of manual and  
748 global estimations (averaging the CI across sections). D) Comparison  
749 of CoV of the manual and global CI.

750 **Figure 7:** Comparison between CoV of manual and automated Caval In-

751 dex (CI) values. Intra- and inter-operator variabilities are considered  
752 (showing the distribution of 10 values, one for each subject, in terms  
753 of median, quartiles and range, plus an outlier shown individually).  
754 The manual CI estimations are the mean of three CI measurements in  
755 M-mode (reflecting the choice of 3 respiration cycles). The automated  
756 CI estimations are given by the mean of all CI measurements obtained  
757 from each video-clip ( $CI_{global}$ , obtained averaging across 3 respiration  
758 cycles and 5 longitudinal sections).

Table 1: ANOVA table considering the CI obtained using either the standard approach (manual CI) or the automated one ( $CI_{global}$ ); DOF - degrees of freedom, RC - respiration cycle.

Source	DOF	Sum of squares		Mean squares		F		p-value	
		<i>manual</i>	<i>global</i>	<i>manual</i>	<i>global</i>	<i>manual</i>	<i>global</i>	<i>manual</i>	<i>global</i>
Subject	9	4.03	2.30	0.45	0.25	29.01	30.01	$\approx 10^{-29}$	$\approx 10^{-29}$
Repetition	1	$6 \cdot 10^{-4}$	0.026	$6 \cdot 10^{-4}$	0.026	0.03	3.03	0.84	0.083
Operator	2	1.05	0.111	0.53	0.055	34.22	6.49	$\approx 10^{-13}$	0.002
RC	2	0.02	$3.5 \cdot 10^{-4}$	0.01	$1.7 \cdot 10^{-4}$	0.67	0.02	0.51	0.98
Error	165	2.54	1.40	0.015	0.008				
Total	179	7.66	3.84						

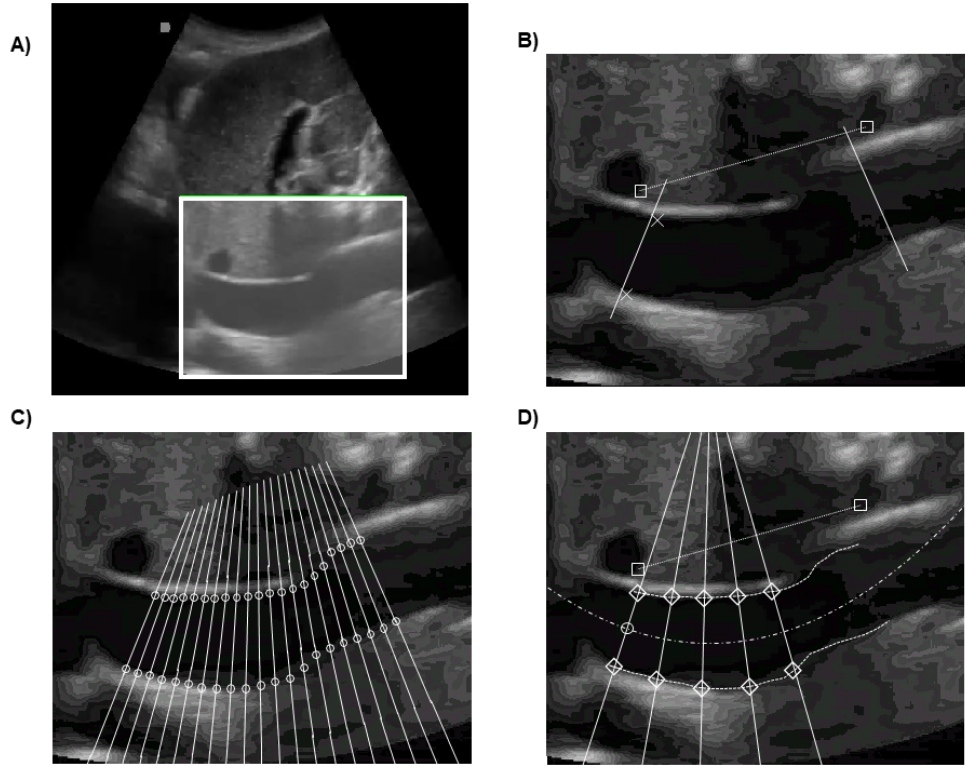


Figure 1: A) Selection of a rectangle including the IVC portion of interest in the first frame of the video-clip. B) Reference points (squares), leftmost and rightmost sections of interest (continuous lines) and points close to the vessel edges along the leftmost section (indicated by X). C) The algorithm computes 21 lines uniformly distributed between the extreme sections indicated in B) and estimates the profile of the vein along them (the estimated border points are indicated with circles). D) From the estimated border of the vessel, the midline is computed and interpolated with a parabola (dash-dot line); five equidistant points are selected on this parabola, starting from the confluence of the hepatic vein in the IVC and new lines perpendicular to it are considered as sections along which to compute the vein diameters (border points indicated with diamonds).

Table 2: Intraclass correlation coefficient (ICC), considering intra- and inter-operators estimates of different caval indexes (manual and automated CI, CCI and RCI, obtained averaging across different sections). Different operators are shown in order of increasing experience (FC less than 1 year, AR 2 years, PP more than 20 years of experience).

	<b>ICC</b>			
<i>Operator</i>	<i>CI standard</i>	<i>CI<sub>global</sub></i>	<i>CCI<sub>global</sub></i>	<i>RCI<sub>global</sub></i>
<b>FC</b>	48.9%	45.3%	61.2%	6.9%
<b>AR</b>	81.7%	46.8%	72.8%	41.0%
<b>PP</b>	77.6%	78.6%	89.5%	70.7%
<b>Inter-operator</b>	61.5%	70.4%	87.5%	49.9%

Table 3: Fisher ratio of estimates of different caval indexes (manual and automated CI, CCI and RCI, obtained averaging across different sections), considering intra- and inter-operator values.

	<b>Fisher ratio</b>			
<i>Operator</i>	<i>CI standard</i>	<i>CI<sub>global</sub></i>	<i>CCI<sub>global</sub></i>	<i>RCI<sub>global</sub></i>
<b>FC</b>	3.20	2.24	2.54	1.43
<b>AR</b>	31.52	2.11	48.83	3.02
<b>PP</b>	9.11	7.34	25.92	9.73
<b>Inter-operator</b>	2.06	8.21	23.52	2.56

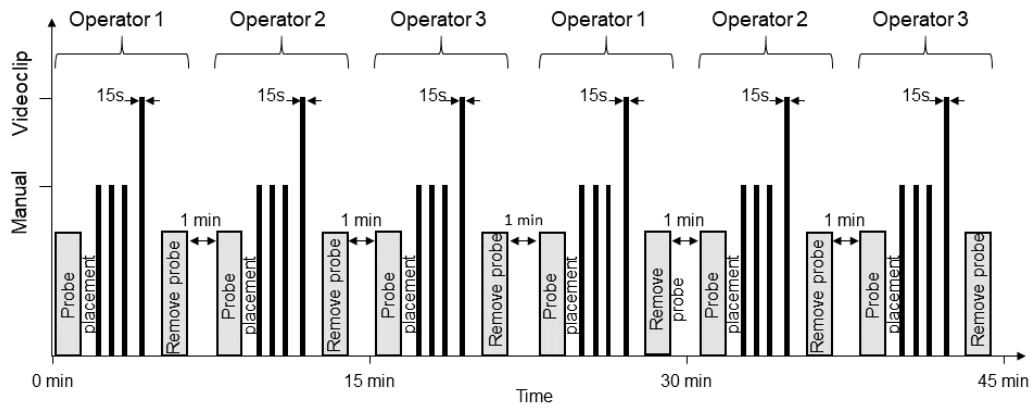


Figure 2: Experimental protocol. Each operator acquired three manual measurements (in M-mode) and then the video (in B-mode). The same procedure was followed twice for each of the three operators.



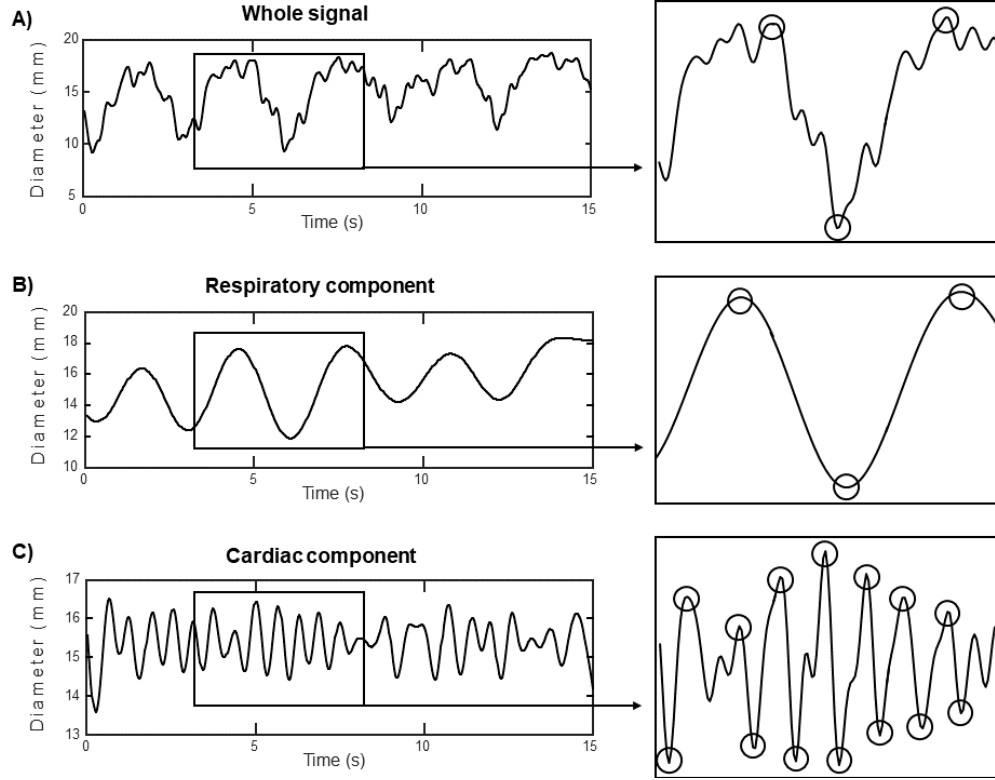


Figure 3: A) Caval index (CI) estimated on the whole signal. The local maxima and minima of the respiratory component are found; then a window of 1 s duration centred on each of these points is explored to find the maxima or minima on the whole signal (indicated with circles). B) Respiratory caval index (RCI), computed on the breath component. This component is isolated with a low pass filter; then, maxima and minima (indicated with circles) are automatically found and used for RCI calculation. C) Cardiac caval index (CCI) computed on the heartbeat component. The component is isolated with a high pass filter; then, its local maxima and minima (indicated with circles) are computed and used for CCI estimation.

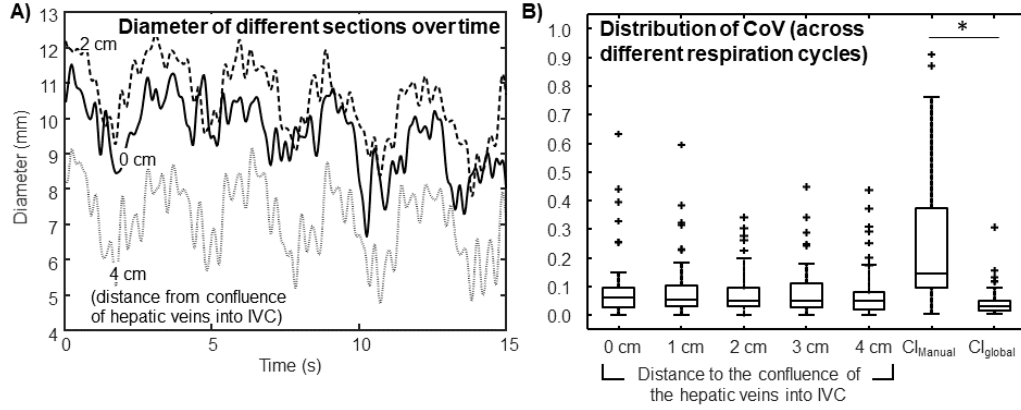


Figure 4: A) Time course of IVC diameter at three different sections simultaneously monitored in a representative subject. B) Distribution of CoV of  $CI_{auto}$ , obtained considering the 6 measurements from all 10 subjects, separately for the five sections and compared with manual CI and  $CI_{global}$ .

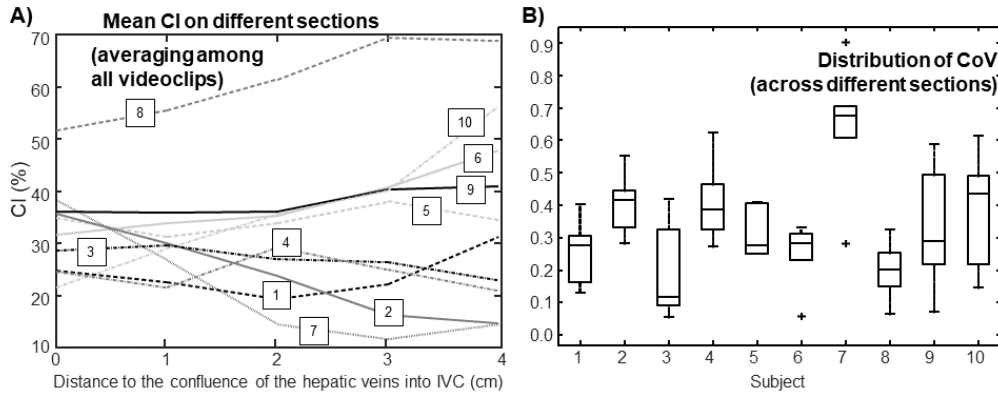


Figure 5: Variation of the Caval Index (CI) when estimated by the automated method at different longitudinal positions, expressed as the distance from the confluence of the hepatic veins. A) Each trace corresponds to one subject (average of all sessions). B) Median, quartiles and range (outliers shown individually) of the coefficient of variation (CoV) of the CI across the 5 sections along the vein, for each subject.

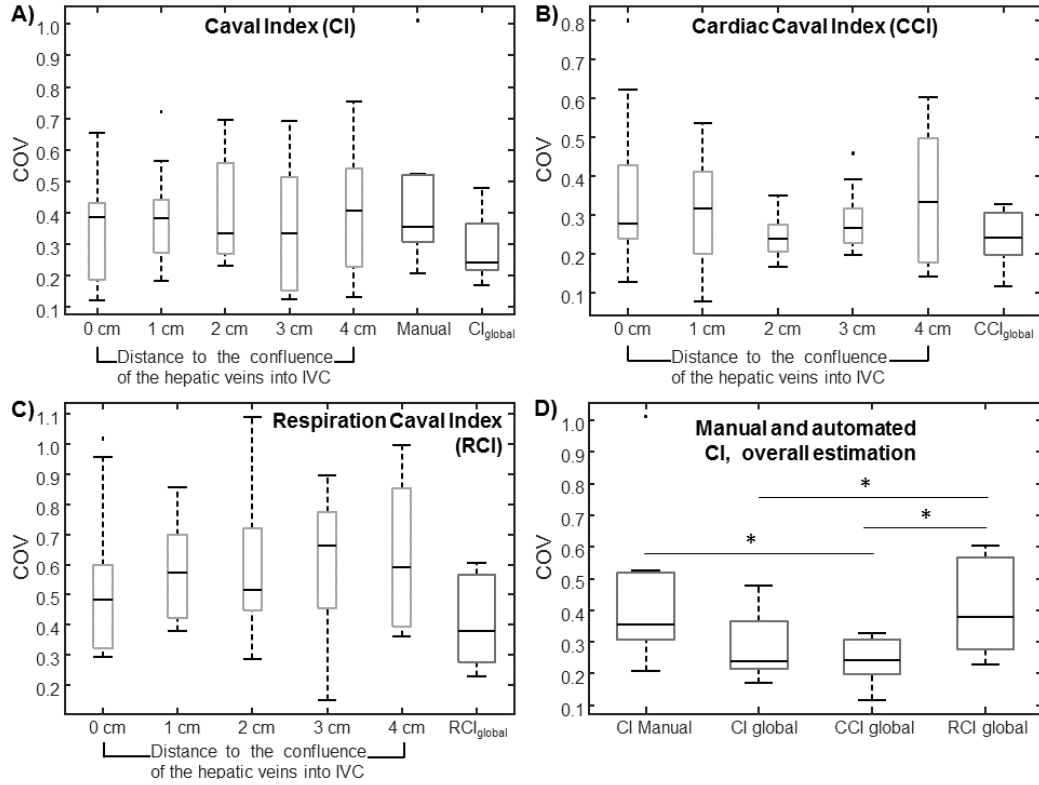


Figure 6: Coefficient of variation (CoV) for each index (manual CI and automated estimation of CI, CCI and RCI) computed across different experimental sessions (median, quartiles and range; outliers shown individually). A), B) and C): CoV of the indexes (CI, CCI and RCI, respectively) extracted at different distances from the confluence of the hepatic vein into the IVC and, to the right, the CoV of manual and global estimations (averaging the CI across sections). D) Comparison of CoV of the manual and global CI.

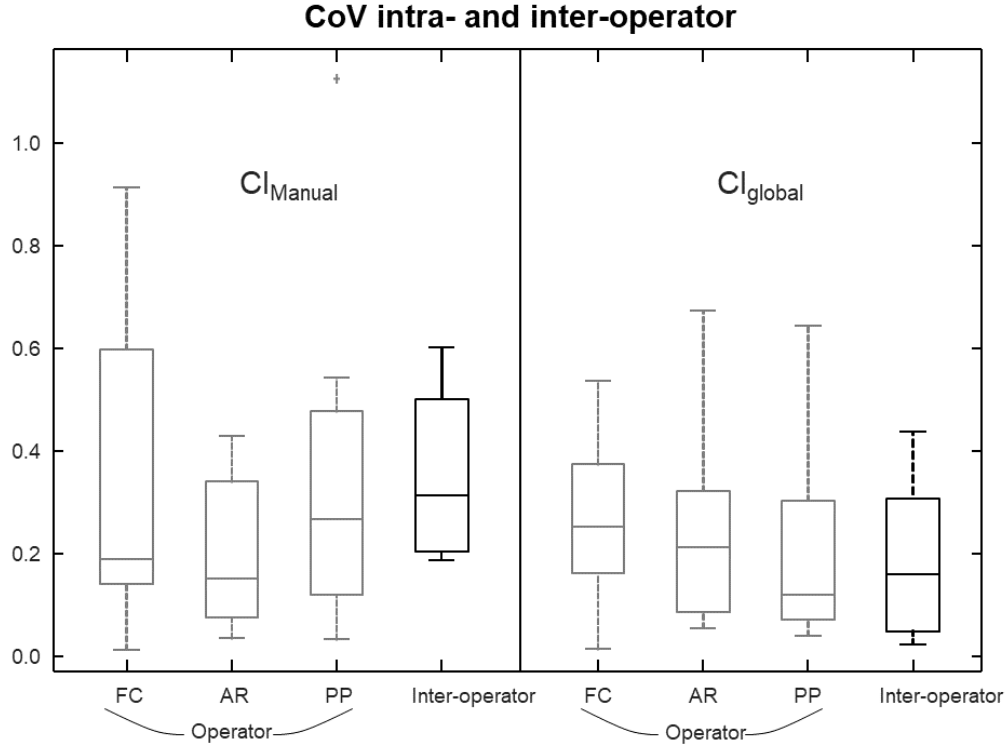


Figure 7: Comparison between CoV of manual and automated Caval Index (CI) values. Intra- and inter-operator variabilities are considered (showing the distribution of 10 values, one for each subject, in terms of median, quartiles and range, plus an outlier shown individually). The manual CI estimations are the mean of three CI measurements in M-mode (reflecting the choice of 3 respiration cycles). The automated CI estimations are given by the mean of all CI measurements obtained from each video-clip ( $CI_{global}$ , obtained averaging across 3 respiration cycles and 5 longitudinal sections).